

Noninvasive estimation of the electrohysterographic action-potential conduction velocity

Citation for published version (APA):

Rabotti, C., Mischi, M., Oei, S. G., & Bergmans, J. W. M. (2010). Noninvasive estimation of the electrohysterographic action-potential conduction velocity. *IEEE Transactions on Biomedical Engineering*, 57(9), 2178-2187. <https://doi.org/10.1109/TBME.2010.2049111>

DOI:

[10.1109/TBME.2010.2049111](https://doi.org/10.1109/TBME.2010.2049111)

Document status and date:

Published: 01/01/2010

Document Version:

Publisher's PDF, also known as Version of Record (includes final page, issue and volume numbers)

Please check the document version of this publication:

- A submitted manuscript is the version of the article upon submission and before peer-review. There can be important differences between the submitted version and the official published version of record. People interested in the research are advised to contact the author for the final version of the publication, or visit the DOI to the publisher's website.
- The final author version and the galley proof are versions of the publication after peer review.
- The final published version features the final layout of the paper including the volume, issue and page numbers.

[Link to publication](#)

General rights

Copyright and moral rights for the publications made accessible in the public portal are retained by the authors and/or other copyright owners and it is a condition of accessing publications that users recognise and abide by the legal requirements associated with these rights.

- Users may download and print one copy of any publication from the public portal for the purpose of private study or research.
- You may not further distribute the material or use it for any profit-making activity or commercial gain
- You may freely distribute the URL identifying the publication in the public portal.

If the publication is distributed under the terms of Article 25fa of the Dutch Copyright Act, indicated by the "Taverne" license above, please follow below link for the End User Agreement:

www.tue.nl/taverne

Take down policy

If you believe that this document breaches copyright please contact us at:

openaccess@tue.nl

providing details and we will investigate your claim.

Noninvasive Estimation of the Electrohysterographic Action-Potential Conduction Velocity

Chiara Rabotti*, Massimo Mischi, S. Guid Oei, and Jan W. M. Bergmans, *Senior Member, IEEE*

Abstract—Electrophysiological monitoring of the fetal-heart and the uterine-muscle activity, referred to as an electrohysterogram, is essential to permit timely treatment during pregnancy. While remarkable progress is reported for fetal-cardiac-activity monitoring, the electrohysterographic (EHG) measurement and interpretation remain challenging. In particular, little attention has been paid to the analysis of the EHG propagation, whose characteristics might be predictive of the preterm delivery. Therefore, this paper focuses, for the first time, on the noninvasive estimation of the conduction velocity of the EHG-action potentials. To this end, multichannel EHG recording and surface high-density electrodes are used. A maximum-likelihood method is employed for analyzing the EHG-action-potential propagation in two dimensions. The use of different weighting strategies of the derived cost function is introduced to deal with the poor signal similarity between different channels. The presented methods were evaluated by specific simulations proving the best weighting strategy to lead to an accuracy improvement of 56.7%. EHG measurements on ten women with uterine contractions confirmed the feasibility of the method by leading to conduction velocity values within the expected physiological range.

Index Terms—Action potentials (APs), conduction velocity (CV), electrohysterography (EHG), electromyography, high density electrodes, maximum likelihood (ML) estimation.

I. INTRODUCTION

THE UNDERSTANDING of risk factors and mechanisms related to preterm labor has been advancing and many public health and medical interventions to reduce the incidence of preterm birth have been introduced. The preterm birth rate has, however, risen in most industrialized countries and it still accounts for 75% of perinatal mortality and more than 50% of long-term morbidity [1], with an associated annual-societal-economic cost that, in the United States alone, was estimated to an amount of 26.2 billion in 2005 [2]. It is well established that

pregnancy-monitoring techniques are essential to assess the key risk factors and permit timely medical intervention; however, accurate prediction of the delivery time, which can be the key parameter for timely treatment of premature labor, still remains a major challenge [3].

Next to fetal-heart-rate monitoring, detection and evaluation of the uterine contractions are of major importance. Typical techniques adopted in clinical practice involve the use of either an external tocodynamometer, which provides a noninvasive indication of contraction onset timing based on external strain gauges, or an internal catheter, which measures the intrauterine-amniotic pressure [3]. Only the latter technique provides quantitative information, but it is invasive and applicable only during labor [3].

In the past few years, a noninvasive alternative technique has been proposed that promises reliable assessment of the uterine activity without the use of intrauterine catheterization. Quantitative information on the myometrium (uterine muscle) is in fact derived from the analysis of its electrical activity, referred to as an electrohysterogram. Several techniques have been proposed for the analysis of the electrohysterographic (EHG) signal. Some authors have developed methods for the noninvasive estimation of the intrauterine pressure [4]–[6], while other authors could distinguish between two different EHG frequency components [7] or observe a shift in the frequency content of the EHG signal as delivery approaches [8], [9], possibly being able to predict the course of pregnancy. The ultimate goal and main challenge remain the prediction of preterm delivery. While the reported techniques are mostly based on single channel measurements [9], we believe that important information for monitoring and predicting the progress of pregnancy resides in the EHG signal propagation characteristics as also suggested in [10] and [11].

Different from skeletal muscles, which are striated and present an anatomical direction of propagation parallel to the fiber orientation, the myometrium is a smooth muscle; as a result, the direction of propagation of the myometrium intracellular action potential (AP), i.e., the electrical activation of the myometrial cells, is *a priori* unknown [7]. The propagation of electrical activity in the myometrium mainly depends, in fact, on the specific pattern of gap-junction connections which are dynamically formed between cells during each contraction [12], [13]. Possible additional parameters that may influence the propagation of uterine APs are calcium waves [14] and the possible bundle arrangement of the myometrium fibers [15].

APs usually occur in bursts. Each burst usually corresponds to a contraction event [16]. The burst frequency and duration as well as the AP frequency within a burst are highly dependent on

Manuscript received November 20, 2009; revised February 5, 2010 and April 13, 2010; accepted April 14, 2010. Date of publication May 10, 2010; date of current version August 18, 2010. This work was supported by the Dutch Technology Foundation, STW. Asterisk indicates corresponding author.

*C. Rabotti is with the Department of Electrical Engineering, Eindhoven University of Technology, Eindhoven 5600MB, The Netherlands (e-mail: c.rabotti@tue.nl).

M. Mischi and J. W. M. Bergmans are with the Department of Electrical Engineering, Eindhoven University of Technology, Eindhoven 5600MB, The Netherlands (e-mail: m.mischi@tue.nl; j.w.m.bergmans@tue.nl).

S. G. Oei is with the Department of Obstetrics and Gynecology, Máxima Medical Center, Veldhoven 5500 MB, The Netherlands, and is also with the Department of Electrical Engineering, Eindhoven University of Technology, Eindhoven, The Netherlands (e-mail: g.oei@mmc.nl).

Digital Object Identifier 10.1109/TBME.2010.2049111

the subject and the parturition stage. In human, the bursts' duration can be more than 1 min [16], with a burst frequency around 0.1 Hz [7]. The AP frequency within a burst has been reported to range between 0.1 and 10 Hz [7], with the majority of studies focusing on the frequency range 0.1–3 Hz [17], [18] and 0.3–1 Hz [8], [11], [16], [19]. Most of the previous literature was dedicated to the analysis of the entire burst and only few studies were dedicated to the analysis of single surface APs [13], [19], [20]. However, *in vitro* studies have demonstrated that, in association with the increase of the gap-junction number, individual APs propagate for longer distance and with higher conduction velocity (CV) at parturition than at preterm [13]. Furthermore, as different APs have different propagation properties even within the same burst, analysis of single AP CV can lead to more detailed information compared to the whole burst analysis.

In this paper, we focus, for the first time, on a method for the estimation of the CV of single surface APs, which are extracted from EHG signals recorded noninvasively on women in labor. By surface AP, we refer to a spike extracted from a single-channel EHG burst that, being recorded noninvasively, is the weighted average of the electrical activity of all the underlying excited cells [21], [22]. An additional novelty of this paper resides in the EHG signal recording methodology, which comprises the use of a high-density (HD) electrode grid. The grid, in fact, integrates a larger number of electrodes (64) with a reduced surface and smaller interelectrode distance with respect to the previous literature [5], [6], [10], [18], [23]. Furthermore, due to *a priori* unknown AP direction of propagation, the bidimensional arrangement of the electrodes on the grid (8×8) permits to estimate all the possible CV directions along the abdominal plane parallel to the abdominal surface.

Several methods are available from the electromyography literature for the measurement of the surface AP CV. Due to the signal source (skeletal muscles), these methods use monodimensional information, as the direction of propagation can be derived from the muscle-fiber orientation. These methods can be divided in four major categories [24]: cross-correlation function maximization [25], phase difference [26], maximum likelihood (ML) [27], and the detection of spectral dips [28]. A four-electrode implementation of this method (multidip) leading to an analytical solution, has been presented in [29], where Farina and Negro mention the possibility of further increase of the number of electrodes. One of the main issues related to the use of the spectral dips is the large variance in their detection, which is due to the variance of the estimated power spectrum [24]. Furthermore, more extensive validation is required before adapting the method to EHG measurement. In particular, due to the varying direction of propagation of the AP, the extension of the spectral multidip method to two dimensions is neither trivial nor practical.

Among the remaining three methods, the phase difference and the ML method, unlike the cross-correlation method, are both implemented in the frequency domain and permit CV measurements that are not limited by the time-sampling rate [24]. Given the EHG frequency content, usually lower than 1 Hz [4], this characteristic is highly desirable, permitting low sampling rates and, therefore, reducing the complexity of the signal anal-

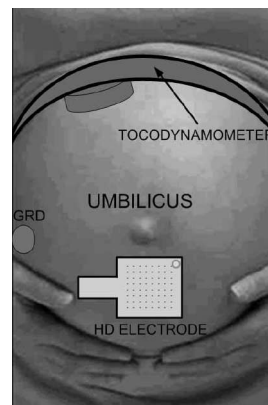


Fig. 1. Scheme of the measurement setup.

ysis. The ML method [30], compared to the phase-difference method, permits a complete exploitation of our multichannel measurements because it allows using all the available acquisition channels, leading to an increased robustness to a low SNR. Furthermore, different from the spectral multidip, the ML method can be easily extended to two dimensions.

The ML method has been, therefore, chosen for the EHG analysis. Due to the models assumed for the AP propagation and for the noise, the ML estimation is equivalent to a mean-square-error minimization. We improved the ML method described in [30] by weighting the derived cost function. A set of weights is automatically determined based on SNR estimates at each channel. Two different weighting approaches are here presented and compared. The method in [30] has been further extended to two dimensions, permitting to estimate amplitude and direction of the CV.

II. METHODOLOGY

In this section, more detailed information is provided on the proposed CV-estimation methods. These methods are based on the characteristics of the measured signals, depending on the measurement system, presented in Section II-A, as well as on the implemented preprocessing steps, presented in Section II-B. The implemented ML method and the proposed improvements are then presented in Section II-C and II-D, respectively.

A. Measurement

After approval of the medical committee of the hospital, ten measurements were performed at the Máxima Medical Center in Veldhoven, The Netherlands, on ten women in labor who signed an informed written consent. The sensors were placed as described in Fig. 1, after skin preparation with an abrasive paste for contact impedance reduction. The EHG signal was recorded by a Refa system (TMS International, Enschede, The Netherlands) comprising a multichannel amplifier for electrophysiological signals and a grid of 64 (8×8) HD electrodes (1 mm diameter, 4 mm interelectrode distance, respectively). The HD electrode grid, whose characteristics are more extensively described in [19], was placed on the midline of the abdomen below the umbilicus; the ground (GRD) electrode was positioned

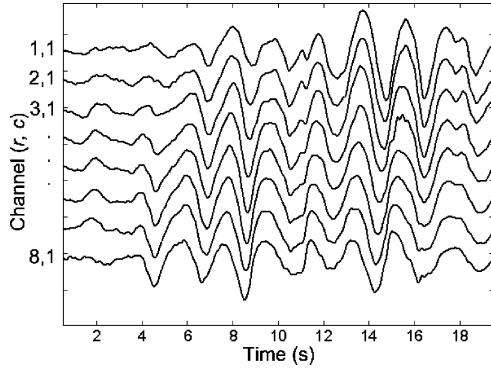


Fig. 2. Example of EHG surface APs recorded by one column of the acquisition matrix after filtering and downsampling.

on the right hip. In order to obtain an efficient rejection of electromagnetic interference, an active GRD electrode was used and all cables were actively shielded [31]. An external tocogram was employed to support the assessment of the contraction period.

B. Data Preprocessing

Given the narrow-band nature of the EHG signal, similar to the previous studies [8], [11], [16], [19], the acquired signals were band-pass filtered by a sixth-order Butterworth filter with low and high cut-off frequencies at 0.1 and 0.8 Hz, respectively. This permitted to suppress most of the noise introduced by the respiration, the maternal electrocardiogram (ECG), and the abdominal electromyogram [19], [32]. The filtered signals could, therefore, be downsampled from 1024 to 16 Hz without introducing aliasing and reducing significantly the computational complexity of the following analysis. This is particularly convenient when dealing with 64 parallel channels. Fig. 2 shows an EHG surface AP sequence registered by one column (eight channels) of the acquisition matrix after filtering and downsampling. In line with the results shown in [20], the example indicates that within the same burst the direction and speed of propagation can vary from one surface AP to the next one. This peculiarity of single-surface APs suggests that their analysis, relative to the whole EHG burst analysis, provides additional and different information that may be of clinical relevance. The expected shape of the EHG surface AP can be derived by the previous studies on the EHG surface AP, where propagating action potentials were directly recorded from the uterus surface [20], and where the EHG surface AP has been measured and modeled [19].

C. Maximum-Likelihood Method

Following the schematic representation of Fig. 3, we assume the EHG to propagate with velocity v and with incidence angle θ ($\theta \in [-\pi, \pi]$) with respect to the vertical axis of the electrode grid. Due to the size of the electrode grid, which is of the order of the signal wavelength [19], we can assume the EHG surface AP to be a planar wave. The signal is detected by N_r rows and N_c columns of electrodes. Assuming that the same signal shape $s(n)$ is measured at each channel, the adopted ML method is developed under the hypothesis that the signal x_{rc} measured

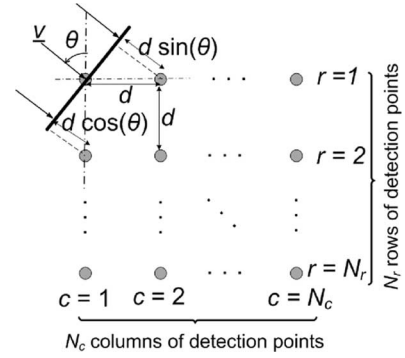


Fig. 3. Schematic description of the system model.

at the channel (r, c) in the r th row ($r \in [1, 2, \dots, N_r]$) and c th column ($c \in [1, 2, \dots, N_c]$) of the electrode grid can be modeled as

$$x_{rc}(n) = s(n - (r - 1)\tau_r - (c - 1)\tau_c) + w_{rc}(n) \quad (1)$$

where n indicates the time sample ($n \in [1, 2, \dots, N]$) and $w_{rc}(n)$ is white Gaussian noise with variance σ_{rc}^2 that is present at channel (r, c) . The choice of the noise model is supported by the narrow band nature of the signal of interest. As from (1), in each channel (r, c) the reference signal shape $s(n)$ is delayed by τ_r and τ_c time samples with respect to the preceding row and column, respectively.

The CV calculation requires the estimation of (τ_r, τ_c) , which can be obtained by the maximization of $p((\tau_r, \tau_c) | x_{rc}(n), s(n))$. Using Bayesian inference and assuming $p(\tau_r, \tau_c)$ uniform, the maximization of $p((\tau_r, \tau_c) | x_{rc}(n), s(n))$ corresponds to the maximization of the probability $p(x_{rc}(n) | (\tau_r, \tau_c), s(n))$ of the samples of the signal $x_{rc}(n)$, given the row and column sample delays τ_r and τ_c and the reference shape $s(n)$, i.e.,

$$p(x_{rc}(n) | (\tau_r, \tau_c), s(n)) = \frac{1}{(2\pi)^{\frac{N}{2}} \sigma_{rc}^N} \cdot e^{-\frac{\sum_{n=1}^N [x_{rc}(n) - s(n - (r-1)\tau_r - (c-1)\tau_c)]^2}{2\sigma_{rc}^2}} \quad (2)$$

Furthermore, the ML estimation of (τ_r, τ_c) corresponds to the maximization of $\ln(p(x_{rc}(n) | (\tau_r, \tau_c), s(n)))$ [33], where

$$\ln(p(x_{rc}(n) | (\tau_r, \tau_c), s(n))) = \ln\left(\frac{1}{(2\pi)^{\frac{N}{2}} \sigma_{rc}^N}\right) - \frac{\sum_{n=1}^N [x_{rc}(n) - s(n - (r-1)\tau_r - (c-1)\tau_c)]^2}{2\sigma_{rc}^2} \quad (3)$$

The expression in (3) can be extended to the entire matrix including all rows r and columns c . The estimation of (τ_r, τ_c) reduces, therefore, to the minimization of the cost function

$$\varepsilon^2(\tau_r, \tau_c) = \sum_{r=1}^{N_r} \sum_{c=1}^{N_c} \sum_{n=1}^N [x_{rc}(n) - s(n - (r-1)\tau_r - (c-1)\tau_c)]^2 \quad (4)$$

Since the signals $x_{rc}(n)$ are only available for discrete values of τ_r and τ_c , minimization of (4) results in a discrete estimate of

the optimum (τ_r, τ_c) , which depends on the sampling rate. By using Parseval's equality, (4) can be transformed in the frequency domain, where τ_r and τ_c become continuous multiplicative factors of the phase and can be estimated without resolution limits. Indicated by $X_{rc}(f)$ and $S(f)$, the Fourier transform of the signal recorded at the channel (r, c) and of the reference shape, respectively, the resulting cost function is

$$E^2(\tau_r, \tau_c) = \frac{2}{N} \sum_{r=1}^{N_r} \sum_{c=1}^{N_c} \sum_{f=1}^{N/2} \left[X_{rc}(f) + S(f) e^{-j2\pi f[(r-1)\tau_r + (c-1)\tau_c]} \right]^2. \quad (5)$$

From the description in Fig. 3, for an interelectrode distance equal to d and a temporal-sampling frequency f_s , it follows that τ_r and τ_c are related to the conduction velocity v and to the incidence angle θ by

$$\begin{aligned} \tau_r &= f_s \frac{d \cos(\theta)}{v} \\ \tau_c &= f_s \frac{d \sin(\theta)}{v}. \end{aligned} \quad (6)$$

The shape function $S(f)$ can be estimated as the average of all the channels $X_{rc}(f)$ after alignment, i.e., in the temporal frequency domain

$$\widehat{S}(f) = \frac{1}{N_c N_r} \sum_{r=1}^{N_r} \sum_{c=1}^{N_c} X_{rc}(f) e^{j2\pi f[(r-1)\tau_r + (c-1)\tau_c]}. \quad (7)$$

The resulting estimated cost function $\widehat{E}^2(\tau_r, \tau_c)$ is then

$$\begin{aligned} \widehat{E}^2(\tau_r, \tau_c) &= \frac{2}{N} \sum_{r=1}^{N_r} \sum_{c=1}^{N_c} \sum_{f=1}^{N/2} \left[X_{rc}(f) + \right. \\ &\quad \left. - \frac{1}{N_r N_c} \sum_{m=1}^{N_r} \sum_{p=1}^{N_c} X_{mp}(f) e^{j2\pi f[(m-r)\tau_r + (p-c)\tau_c]} \right]^2. \end{aligned} \quad (8)$$

D. Channel Weighting

The model in (1) is based on the assumption that the signals recorded at different channels are delayed versions of the same reference shape $s(n)$. This assumption, already weak for skeletal muscles [27], is even weaker for the myometrium, where differences in the volume conductor and cell-to-cell conduction path underneath the electrodes may cause shape variations of the propagating APs [7]. In (1), such shape variations are accounted for by the noise term $w_{rc}(n)$. In order to increase the robustness of the CV estimation to surface AP shape variations due to the presence of noise, the method is improved by introducing proper weights, $a_{rc} \in \mathbb{R}^+$, in the cost function. The resulting weighted

cost function $\widehat{E}_a^2(\tau_r, \tau_c)$ is defined as

$$\begin{aligned} \widehat{E}_a^2(\tau_r, \tau_c) &= \frac{2}{N} \sum_{r=1}^{N_r} \sum_{c=1}^{N_c} \sum_{f=1}^{N/2} \left[a_{rc} \left(X_{rc}(f) \right. \right. \\ &\quad \left. \left. - \widehat{S}(f) e^{-j2\pi f[(r-1)\tau_r + (c-1)\tau_c]} \right) \right]^2. \end{aligned} \quad (9)$$

The weights are chosen to be inversely proportional to the standard deviation of the channel noise σ_{rc} [34], i.e.,

$$a_{rc} = \frac{A}{\sigma_{rc}} = \frac{A}{\frac{2}{N} \sqrt{\sum_{f=1}^{N/2} |W_{rc}(f)|^2}} \quad (10)$$

where A indicates a proper scaling factor to normalize the weight sum to 1. For the expression of a_{rc} in the frequency domain, last term of (10), Parseval's equality is used, where $|W_{rc}(f)|^2$ is the noise power spectrum in the considered channel (r, c) .

In order to obtain an estimate of the noise power for the generic channel (r, c) , the model in (1) is expressed in the temporal frequency domain f as

$$X_{rc}(f) = S(f) e^{-j2\pi f[(r-1)\tau_r + (c-1)\tau_c]} + W_{rc}(f). \quad (11)$$

By assuming the reference shape $S(f)$ and the noise $W_{rc}(f)$ to be uncorrelated, the noise can be estimated from

$$\sum_{f=1}^{N/2} X_{rc}(f) X_{rc}^*(f) = \sum_{f=1}^{N/2} S(f) S^*(f) + \sum_{f=1}^{N/2} |W_{rc}(f)|^2 \quad (12)$$

where $(\cdot)^*$ is the conjugate operator. The noise power derived by (12) can then be substituted in (10) to provide the weights

$$a_{rc} = \frac{A}{\frac{2}{N} \sqrt{\sum_{f=1}^{N/2} (X_{rc}(f) X_{rc}^*(f) - S(f) S^*(f))}}. \quad (13)$$

The shape $\widehat{S}(f)$ defined in (7) as the average of the aligned signals X_{rc} , which is used as an estimate of the reference signal $\widehat{S}(f)$ in (9), can be employed in (13).

Alternatively, the estimate $\widehat{S}_w(f)$ of the reference shape $S(f)$ in (13) can be calculated as the weighted average of the signals $X_{rc}(f)$, i.e.,

$$\widehat{S}_w(f) = \sum_{r=1}^{N_r} \sum_{c=1}^{N_c} a_{rc}^w X_{rc}(f) e^{j2\pi f[(r-1)\tau_r + (c-1)\tau_c]}. \quad (14)$$

Using $\widehat{S}_w(f)$ as an estimate of $S(f)$ in (13), the alternative channel weights a_{rc}^w are defined as

$$a_{rc}^w = \frac{A}{\frac{2}{N} \sqrt{\sum_{f=1}^{N/2} X_{rc}(f) X_{rc}^*(f) - \widehat{S}_w(f) \widehat{S}_w^*(f)}} \quad (15)$$

and using (14) for $\widehat{S}_w(f)$ and $\widehat{S}_w^*(f)$, (15) can be expressed as, (16), shown at the bottom of the page.

$$a_{rc}^w = \frac{A}{\frac{2}{N} \sqrt{\sum_{f=1}^{N/2} X_{rc}(f) X_{rc}^*(f) - \sum_{r=1}^{N_r} \sum_{c=1}^{N_c} (a_{rc}^w)^2 X_{rc}(f) X_{rc}^*(f)}}. \quad (16)$$

TABLE I
COST FUNCTIONS AND WEIGHTING STRATEGIES

Cost function	Weights	Reference shape
$\hat{E}^2(\tau_r, \tau_c) = \frac{2}{N} \sum_{r=1}^{N_r} \sum_{c=1}^{N_c} \sum_{f=1}^{N/2} \left(X_{rc}(f) - \hat{S}(f) e^{-j2\pi f[(r-1)\tau_r + (c-1)\tau_c]} \right)^2$	N/A	$\hat{S}(f) = \frac{1}{N_r N_c} \sum_{r=1}^{N_r} \sum_{c=1}^{N_c} X_{rc}(f) e^{j2\pi f[(r-1)\tau_r + (c-1)\tau_c]}$
$\hat{E}_a^2(\tau_r, \tau_c) = \frac{2}{N} \sum_{r=1}^{N_r} \sum_{c=1}^{N_c} \sum_{f=1}^{N/2} \left[a_{rc} \left(X_{rc}(f) - \hat{S}(f) e^{-j2\pi f[(r-1)\tau_r + (c-1)\tau_c]} \right) \right]^2$	$a_{rc} = \frac{A}{\frac{2}{N} \sqrt{\sum_{f=1}^{N/2} (X_{rc}(f) \cdot X_{rc}^*(f) - \hat{S}(f) \cdot \hat{S}^*(f))}}$	$\hat{S}(f) = \frac{1}{N_r N_c} \sum_{r=1}^{N_r} \sum_{c=1}^{N_c} X_{rc}(f) e^{j2\pi f[(r-1)\tau_r + (c-1)\tau_c]}$
$\hat{E}_{a^w}^2(\tau_r, \tau_c) = \frac{2}{N} \sum_{r=1}^{N_r} \sum_{c=1}^{N_c} \sum_{f=1}^{N/2} \left[a_{rc}^w \left(X_{rc}(f) - \hat{S}_w(f) e^{-j2\pi f[(r-1)\tau_r + (c-1)\tau_c]} \right) \right]^2$	$a_{rc}^w = \frac{A}{\frac{2}{N} \sqrt{\sum_{f=1}^{N/2} (X_{rc}(f) \cdot X_{rc}^*(f) - \hat{S}_w(f) \cdot \hat{S}_w^*(f))}}$	$\hat{S}_w(f) = \sum_{r=1}^{N_r} \sum_{c=1}^{N_c} a_{rc}^w X_{rc}(f) e^{j2\pi f[(r-1)\tau_r + (c-1)\tau_c]}$

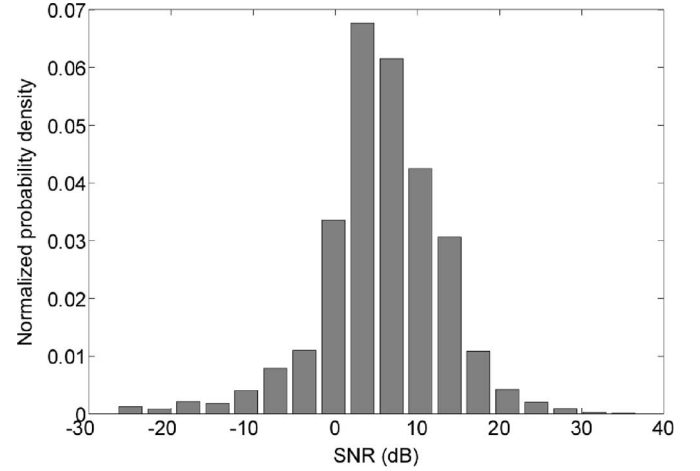


Fig. 4. SNR distribution of 40 APs randomly selected from ten patients.

The $N_r N_c$ equations are of the same form as (16), which holds for each channel (r, c) , and the condition on the weight sum

$$\sum_{r=1}^{N_r} \sum_{c=1}^{N_c} a_{rc}^w = 1 \quad (17)$$

lead to a system of $(N_r N_c) + 1$ linearly independent equations, where the $N_r N_c$ unknown weights and the scaling factor A can be univocally derived. Using the same weights a_{rc}^w for the cost function and the reference shape in (13) leads to the following expression of the estimated alternative cost function $\hat{E}_{a^w}^2(\tau_r, \tau_c)$

$$\hat{E}_{a^w}^2(\tau_r, \tau_c) = \frac{2}{N} \sum_{r=1}^{N_r} \sum_{c=1}^{N_c} \sum_{f=1}^{N/2} \left[a_{rc}^w \left(X_{rc}(f) + \hat{S}_w(f) e^{-j2\pi f[(r-1)\tau_r + (c-1)\tau_c]} \right) \right]^2 \quad (18)$$

where differently from the cost function $E^2(\tau_r, \tau_c)$ in (9), the weights a_{rc}^w are calculated using the weighted average $\hat{S}_w(f)$ of the signals $X_{rc}(f)$ as an estimate of the reference shape $S(f)$.

For validation, the three cost functions $E^2(\tau_r, \tau_c)$, $E_a^2(\tau_r, \tau_c)$, and $\hat{E}_{a^w}^2(\tau_r, \tau_c)$, whose definitions are summarized in Table I, were compared on simulated and real signals. In our previous study [35], the use of clustering in combination with weighting was successfully proposed, for the first time, to select a subset of electrodes for the CV estimation in one direction and to improve the estimate accuracy. In the present study, we tested the combined use of clustering and weighting by defining the cluster distance as the reciprocal of the weights a_{rc}^w .

For the minimization of the cost functions, the Nelder–Mead Simplex search method was used [36]. The values of τ_r and τ_c are initialized according to the average values reported in the literature for the uterine AP CV in the circumferential direction (2.8 cm/s) and in the longitudinal direction (6.8 cm/s), respectively [20]. The proposed methods were implemented in MATLAB (Mathworks). For each surface AP, with the algorithm running on an Intel Core2 Duo Processor with 1.97 GB RAM, the CV estimate was obtained in about 1 min.

TABLE II
STANDARD DEVIATION OF THE DELAY ESTIMATES FOR DIFFERENT VELOCITIES AND ANGLES OF INCIDENCE

v= 4cm/s								
Cost Function	$\theta = 0$		$\theta = \pi/12$		$\theta = \pi/6$		$\theta = \pi/4$	
	SD _r	SD _c	SD _r	SD _c	SD _r	SD _c	SD _r	SD _c
$\widehat{E}^2(\tau_r, \tau_c)$	7.0 ms	5.5 ms	6.2 ms	5.4 ms	6.2 ms	5.9 ms	6.4 ms	5.6 ms
$\widehat{E}_d^2(\tau_r, \tau_c)$	3.2 ms	2.5 ms	3.0 ms	2.8 ms	2.9 ms	3.0 ms	3.0 ms	3.1 ms
$\widehat{E}_{d^w}^2(\tau_r, \tau_c)$	2.7 ms	2.3 ms	2.5 ms	2.4 ms	2.5 ms	2.5 ms	2.7 ms	2.6 ms
v= 10cm/s								
Cost Function	$\theta = 0$		$\theta = \pi/12$		$\theta = \pi/6$		$\theta = \pi/4$	
	SD _r	SD _c	SD _r	SD _c	SD _r	SD _c	SD _r	SD _c
$\widehat{E}^2(\tau_r, \tau_c)$	4.5 ms	4.2 ms	4.1 ms	3.7 ms	3.8 ms	3.5 ms	3.7 ms	3.5 ms
$\widehat{E}_d^2(\tau_r, \tau_c)$	2.9 ms	2.3 ms	2.7 ms	2.1 ms	2.6 ms	2.2 ms	2.4 ms	2.3 ms
$\widehat{E}_{d^w}^2(\tau_r, \tau_c)$	2.0 ms	1.9 ms	1.8 ms	1.7 ms	1.6 ms	1.6 ms	1.6 ms	1.6 ms

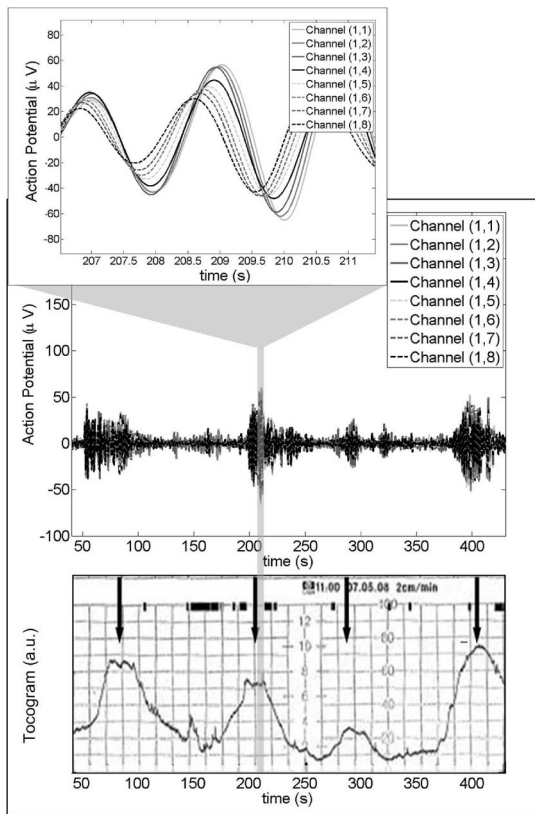


Fig. 5. Example of EHG bursts and corresponding tocogram. An example of selected surface AP is also shown in the top of the figure by magnifying a time segment of the burst at the contraction peak.

III. RESULTS

A. Simulated Signals

The presented CV-estimation methods are evaluated by means of simulations based on real signals. A time interval of 10 s including a complete EHG surface AP was extracted from real EHG recording to obtain the reference shape $s(n)$. This signal was then artificially delayed to simulate the measurement of the same surface AP by the other electrodes on the grid. Two arbitrary velocities of 4 and 10 cm/s and four different angles of incidence, equal to 0, $\pi/12$, $\pi/6$, and $\pi/4$, were considered.

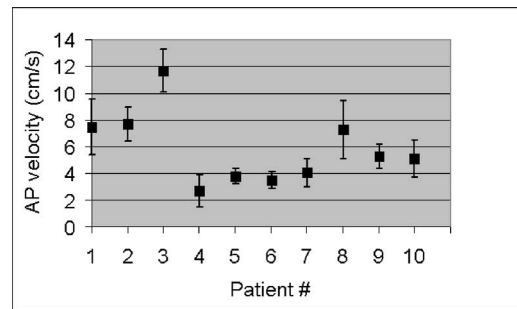


Fig. 6. Mean and standard deviations of the CV amplitude for all patients.

After downsampling at 16 Hz, the delays corresponded to a fraction of the sampling frequency.

White Gaussian noise was then added to the reference shape signal to simulate the remaining 63 channels. In order to determine a realistic SNR, 40 APs (four per subject) were selected from the available recorded signals. The SNR was estimated by (12) in each channel. The distribution of the SNR expressed in dB over the forty 64-channel recordings, (see Fig. 4), resulted well represented by a Gaussian probability density function (correlation coefficient $R = 0.97$ with the Gaussian fit), with mean and standard deviations equal to 5.88 and 7.41 dB, respectively. Therefore, for each simulated velocity and angle of incidence, 1000 different noise sequences were generated and added to each channel; the SNR was randomly distributed among the channels according to a Gaussian probability density function with the same mean and standard deviation estimated from the real signals.

The 64-channel simulations were then used to evaluate the different methods for the CV estimation. The CV estimates were calculated by the ML method alone, and after the use of the two different weighting strategies in Table I. The standard deviations of the error for the row delay τ_r (SD_r) and the column delay τ_c (SD_c) are reported in Table II for each simulated angle of incidence and for the different used cost functions. The maximum mean error was lower than 5% of the reference value of delay. On average, weighting the cost function reduced the standard deviation of the error by 44.06% \pm 8.03%.

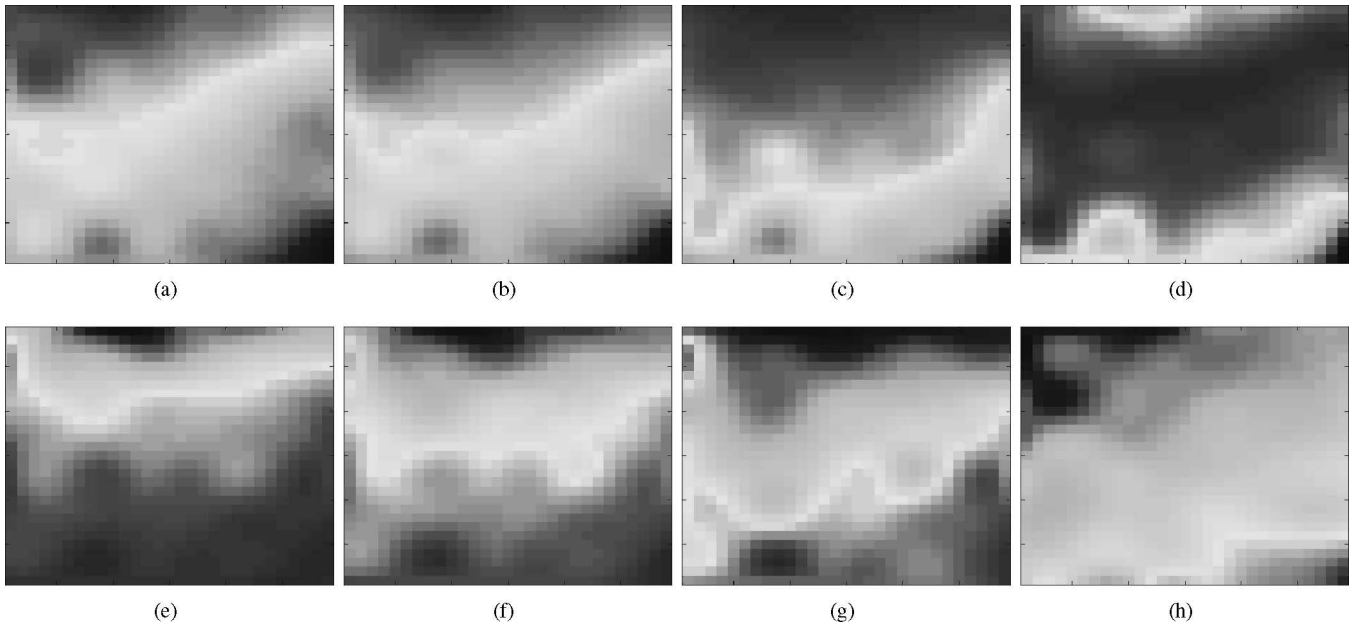


Fig. 7. Temporal sequence of surface AP propagation maps as recorded by the whole 64-channel electrode grid after spatial interpolation. The local amplitude of the surface AP is proportional to the gray level of the map. The reported maps, from (a) to (h), were recorded every 100 ms.

Weighting both the cost function and the reference shape provided an average improvement of $56.70\% \pm 2.25\%$.

B. Real Signals

The measurement feasibility was also tested on ten women between the 38th and the 41st weeks of gestation with uterine contractions. Nine women were classified to be in labor (dilatation > 3 cm) and delivered within 13 h from the EHG recording. During contractions, time segments were visually inspected and two surface APs were determined per each woman around the contraction peak. In Fig. 5, an example recording of EHG bursts after preprocessing and the associated tocographic signal are shown. The figure shows that the amplitude during the quiescent period is significantly lower than during the activity burst. The magnified time segment in Fig. 5 shows that the surface AP propagates along the recording electrodes with a velocity of few centimeter per second. This suggests that the selected waveform originates from uterine activity and not from artifacts due to motion, which typically do not propagate, or to the ECG, which is not expected to show propagation along electrodes placed on the abdomen. The longer duration of surface APs relative to the internal measurements reported in the literature [20] can be explained by the effect of the volume conductor [19] and by the fact that the signal recorded by each surface electrode is the weighted average of the electrical activity of all the underlying excited cells [21], [22].

The surface AP visual selection aimed at excluding possible circulating excitations and re-entries [37]. Surface APs originating in the middle of the electrode grid and then propagating in two different directions or not propagating through the entire electrode were also excluded. Only those surface APs origi-

nating outside or on the border of the electrode grid and then propagating through the entire electrode grid were selected.

The method comprising the minimization of the cost function $\hat{E}_{aw}^2(\tau_r, \tau_c)$ was applied on the entire 8×8 electrode matrix. The average and standard deviation of the velocity amplitude are reported in Fig. 6 for all patients. On average, we found vertical and horizontal components of the velocity amplitude equal to 3.68 ± 3.24 and 3.76 ± 3.21 cm/s, respectively. These estimates are within the expected physiological range [7]. Concerning the wave-incidence angle, as was earlier demonstrated by *in-vitro* studies, a preferred direction of propagation of single AP could not be highlighted and, even within the same contraction, different incidence angles were detected for different APs.

An example of surface AP propagation is shown in Fig. 7, by means of a temporal sequence of spatial maps, representing the electrode grid; the local amplitude of the recorded surface AP is proportional to the gray level of the map. Therefore, the dark region represents the depolarization phase of the surface AP. In the first four maps, the repolarization phase of the preceding surface AP (light region) is also visible. The reported maps refer to 8 different instants, 1 every 100 ms, of the surface AP propagation. In the presented example, the surface AP propagates with an incidence angle of about 6° and a velocity of 4 cm/s, as detected by the proposed method.

IV. DISCUSSION AND CONCLUSION

There are only few studies dedicated to the EHG signal propagation properties by multichannel recordings [10], [11]. These studies investigated the propagation on a large scale by analyzing the EHG bursts on the whole uterine muscle. A similar approach has also been attempted by multichannel tocography [38]. On the contrary, this paper focuses on the CV

estimation of single APs. The surface AP CV is an additional parameter of potential clinical relevance. As on a large scale this parameter cannot be accurately derived [11], the propagation analysis is here carried out on a small scale using an HD-electrode grid. This small-scale analysis provides local propagation parameters that can fundamentally contribute, possibly in combination to the global parameters derived by large-scale analysis, to the development of diagnostic and prognostic tools for uterine contraction monitoring and labor prediction.

The measurement of the EHG surface AP CV is here proposed for the first time. The use of an electrode matrix permits estimating the CV vector in two dimensions. This is an important aspect in EHG measurements because, different from the electromyographic CV measurements, the EHG CV direction is not known *a priori*. For the signal analysis, we propose an ML method, which is implemented in two dimensions and comprises the use of weights in the cost function. The weight values depend on the estimated SNR.

Results, on the simulated signals, show that the estimate accuracy is significantly improved by the use of weights. Among the two different weighting strategies that were proposed, the use of the same weights for estimating the reference signal shape and for the cost function results in more accurate estimates. As compared to the ML method alone, on average, the error variance diminished by 56.70%, becoming up to less than 3% of the measured value.

In our previous study [35], the use of clustering in combination with weighting was successfully proposed, for the first time, to select a subset of electrodes for the CV estimation in one direction and to improve the estimate accuracy. In the present study, we tested the combined use of clustering and weighting by defining the cluster distance as the reciprocal of the weights a_{rc}^w . On our simulated signals, the combined use of clustering and weighting led to an estimate accuracy comparable to that of the best weighting strategy (i.e., the use of the cost function $\hat{E}_{a^w}^2(\tau_r, \tau_c)$) alone. As the clustering can be viewed as a form of binary weighting, these results could be expected and are, therefore, not explicitly reported.

The method feasibility was confirmed by measurements on ten women at term with uterine contractions. Calculation of the CV amplitude led to values that are within the expected physiological range [7], [13], [20]. As for the incidence angle of propagating surface AP, different from what is reported for the propagation of the whole electrical burst [11], we could not highlight a most frequent direction of the surface AP propagation pattern even within the same contraction. The same variability in both origin and direction of the surface AP propagation pattern has been previously observed in *in-vivo* and *in-vitro* studies on the uterus, and, at least during labor [20], it seems physiological.

For practical reasons, the real-signal analysis was conducted on APs that were previously selected around the contraction peak in order to exclude waves originating within the electrode area and then propagating in two different directions below the electrode grid. Noteworthy, the proposed method for the CV estimation is not limited by this assumption. In fact, if the surface AP originates within the region covered by the electrode grid and then propagates in two different directions [20], an additional

step is required for detecting the pacemaker electrode (i.e., the first electrode recording the burst). The CV can be estimated for the two directions of propagation by applying the proposed method separately on the two subsets of electrodes in which the grid can be divided by the pacemaker electrode.

Additional exclusion criteria for the surface AP selection were circulating excitation, re-entries, and partial propagation along the electrode grid. These phenomena have been previously observed for the myometrium activity in animal studies. In particular, in rats circulating excitation had an occurrence of 22% [37]. Partial propagation of the surface AP along the electrode grid are common events especially at the beginning or at the end of a burst as highlighted in [39], where only in 25% of the bursts, the mapped area was completely activated by the first AP. As confirmed in the literature, the high probability of these events, which we all excluded from the real-signal analysis, imposed a limitation to the amount of analyzed signals.

The advantage of using an HD 2-D grid for the EHG signal recording is highlighted by the reported sequence of propagation maps. Furthermore, the example of surface AP in the maps satisfies the planar-wave approximation that we assumed in our propagation model.

In conclusion, our results show that the proposed ML method is suitable for the 2-D estimation of the EHG surface AP conduction velocity. Moreover, the use of weights for both the reference shape and the cost function leads to more accurate estimates than the use of the ML alone and should, therefore, be preferred. However, even if conceived for estimating the CV of surface AP extracted from the EHG signal, the proposed method can be employed for the analysis of other types of signal, in particular, when the direction of propagation is *a priori* unknown.

For EHG surface AP analysis, the method, as currently presented, requires an accurate detection of the surface AP as prerequisite for the signal analysis. Future research will focus on implementation and clinical evaluation aspects such as the possibility of automatically selecting surface APs. In general, this work opens new possibilities for future clinical studies aimed at assessing the CV-vector dynamics and its value for analysis of the pregnancy course and, most importantly, for prediction of preterm delivery.

REFERENCES

- [1] R. Goldenberg, J. Culhane, J. Jams, and R. Romero, "Epidemiology and causes of preterm birth," *Lancet*, vol. 371, pp. 75–84, 2008.
- [2] R. Behrman and A. Butler, *Preterm Birth: Causes, Consequences, and Prevention*. Washington, DC: The National Academy Press, 2007.
- [3] R. Garfield, H. Maul, L. Shi, W. Maner, C. Fittkow, G. Olsen, and G. Saade, "Methods and devices for the management of term and preterm labor," *Ann. NY Acad. Sci.*, vol. 943, pp. 203–224, 2001.
- [4] C. Rabotti, M. Mischi, J. van Laar, S. Oei, and J. Bergmans, "Estimation of internal uterine pressure by joint amplitude and frequency analysis of electrohysterographic signals," *Physiol. Meas.*, vol. 29, pp. 829–841, 2008.
- [5] M. Skowronski, J. Harris, D. Marossero, R. Edwards, and T. Euliano, "Prediction of intrauterine pressure from electrohysterography using optimal linear filtering," *IEEE Trans. Biomed. Eng.*, vol. 53, no. 10, pp. 1983–1989, Oct. 2006.
- [6] J. Jezewski, K. Horoba, and A. Matonia, J. Wrobel, "Quantitative analysis of contraction patterns in electrical activity signal of pregnant uterus as

- alternative to mechanical approach," *Physiol. Meas.*, vol. 26, pp. 753–767, 2005.
- [7] D. Devedeux, C. Marque, S. Mansour, G. Germain, and J. Duchêne, "Uterine electromyography: A critical review," *Amer. J. Obstet. Gynecol.*, vol. 169, pp. 1636–1653, 1993.
- [8] W. Maner, R. Garfield, H. Maul, G. Olson, and G. Saade, "Predicting term and preterm delivery with transabdominal uterine electromyography," *Obstet. Gynecol.*, vol. 101, pp. 1254–1260, 2003.
- [9] M. Vinken, C. Rabotti, S. Oei, and M. Mischi, "Accuracy of frequency-related parameters of the electrohysterogram for predicting preterm delivery: A review of the literature," *Obstet. Gynecol. Surv.*, vol. 64, pp. 529–541, 2009.
- [10] T. Euliano, D. Marossero, M. Nguyen, N. Euliano, J. Principe, and R. Edwards, "Spatiotemporal electrohysterography patterns in normal and arrested labor," *Amer. J. Obstet. Gynecol.*, vol. 200, pp. 54.e1–54.e7, 2009.
- [11] C. Rabotti, M. Mischi, J. van Laar, S. Oei, and J. Bergmans, "Inter-electrode delay estimators for electrohysterographic propagation analysis," *Physiol. Meas.*, vol. 30, pp. 745–761, 2009.
- [12] R. E. Garfield, S. Sims, and E. E. Daniel, "Gap junctions: Their presence and necessity in myometrium during parturition," *Science*, vol. 198, pp. 958–960, 1977.
- [13] S. Miller, R. Garfield, and E. Daniel, "Improved propagation in myometrium associated with gap junctions during parturition," *Amer. J. Physiol. Cell. Physiol.*, vol. 256, pp. C130–C141, 1989.
- [14] R. Young, "Tissue-level signaling and control of uterine contractility: The action potential-calcium wave hypothesis," *J. Soc. Gynecol. Invest.*, vol. 7, pp. 146–152, 2000.
- [15] T. Chard and J. Grudzinskas, *The Uterus*. Cambridge, U.K.: Cambridge Univ. Press, 1994.
- [16] R. Garfield, W. Maner, L. MacKay, D. Schlembach, and G. Saade, "Comparing uterine electromyography activity of antepartum patients versus term labor patients," *Amer. J. Obstet. Gynecol.*, vol. 193, pp. 23–29, 2005.
- [17] H. Leman, C. Marque, and J. Gondry, "Use of the electrohysterogram signal for characterization of contractions during pregnancy," *IEEE Trans. Biomed. Eng.*, vol. 46, no. 10, pp. 1222–1229, Oct. 1999.
- [18] C. Marque, J. Duchêne, S. Leclercq, G. Panczer, and J. Chaumont, "Uterine EHG processing for obstetrical monitoring," *IEEE Trans. Biomed. Eng.*, vol. BME-33, no. 12, pp. 1182–1187, Dec. 1986.
- [19] C. Rabotti, M. Mischi, L. Beulen, S. Oei, and J. Bergmans, "Modeling and identification of the electrohysterographic volume conductor by high-density electrodes," *IEEE Trans. Biomed. Eng.*, vol. 57, no. 3, pp. 519–527, Mar. 2010.
- [20] W. Lammers, H. Mirghani, B. Stephen, S. Dhanasekaran, A. Wahab, and M. Al Sultan, "Patterns of electrical propagation in the intact guinea pig uterus," *Amer. J. Physiol. Regul. Integr. Comp. Physiol.*, vol. 294, pp. R919–R928, 2008.
- [21] M. Zwarts and D. Stegeman, "Multichannel surface EMG: Basic aspects and clinical utility," *Muscle Nerve*, vol. 28, pp. 1–17, 2003.
- [22] J. van Dijk, D. Stegeman, M. Lapatki, and B.G. and Zwarts, "Evidence of potential averaging over the finite surface of a bioelectric electrode using high-density EMG," in *Proc. XVI Congr. ISEK*, 2006, p. 62.
- [23] G. Wolfs and M. van Leeuwen, "Electromyographic observations on the human uterus during labour," *Acta Obstet. Gynecol. Scand.*, vol. 58, pp. 1–61, 1979.
- [24] D. Farina and R. Merletti, "Methods for estimating muscle fibre conduction velocity from surface electromyographic signals," *Med. Biol. Eng. Comput.*, vol. 42, pp. 432–445, 2004.
- [25] P. Parker and R. Scott, "Statistics of the myoelectric signal from monopolar and bipolar electrodes," *Med. Biol. Eng.*, vol. 11, pp. 591–596, 1973.
- [26] I. Hunter, R. Kearney, and L. Jones, "Estimation of the conduction velocity of muscle action potentials using phase and impulse response function techniques," *Med. Biol. Eng.*, vol. 25, pp. 121–126, 1987.
- [27] D. Farina, W. Muhammad, E. Fortunato, O. Meste, R. Merletti, and H. Rix, "Estimation of single motor unit conduction velocity from surface electromyogram signals detected with linear electrode arrays," *Med. Biol. Eng. Comput.*, vol. 39, pp. 225–236, 2001.
- [28] P. Lynn, "Direct on-line estimation of muscle fiber conduction velocity by surface electromyography," *IEEE Trans. Biomed. Eng.*, vol. BME-26, no. 10, pp. 564–571, Oct. 1979.
- [29] D. Farina and F. Negro, "Estimation of muscle fiber conduction velocity with a spectral multidip approach," *IEEE Trans. Biom. Eng.*, vol. 54, no. 9, pp. 1583–1589, Sep. 2007.
- [30] D. Farina and R. Merletti, "Estimation of average muscle fiber conduction velocity from two-dimensional surface EMG recordings," *J. Neurosci. Methods*, vol. 134, pp. 199–208, 2004.
- [31] A. M. van Rijn, A. Peper, and C. Grimbergen, "High-quality recording of bioelectric events. Part 1: Interference reduction, theory and practice," *Med. Biol. Eng. Comput.*, vol. 28, pp. 389–397, 1990.
- [32] W. Maner and R. Garfield, "Identification of human term and preterm labor using artificial neural networks on uterine electromyography data," *Ann. NY Acad. Sci.*, vol. 35, pp. 465–473, 2007.
- [33] C. Bishop, *Pattern Recognition and Machine Learning*. New York: Springer-Verlag, 2006.
- [34] D. Manolakis, V. Ingle, and S. Kogon, *Statistical and Adaptive Signal Processing*. Norwood, MA: Artech House, 2005.
- [35] M. Mischi, C. Rabotti, L. Vosters, S. Oei, and J. Bergmans, "Electrohysterographic conduction velocity estimation," in *Proc. IEEE EMBS Int. Conf.*, 2009, pp. 6934–6939.
- [36] J. Lagarias, J. Reeds, M. Wright, and P. Wright, "Convergence properties of the Nelder-Mead simplex method in low dimensions," *SIAM J. Optim.*, vol. 9, pp. 112–147, 1998.
- [37] W. Lammers, "Circulating excitations and re-entry in the pregnant uterus," *Eur. J. Physiol.*, vol. 433, pp. 287–293, 1997.
- [38] L. Spätling, F. Fallenstein, R. Danders, and A. Hasenburger, "External four-channel tocography during delivery," *Int. J. Gynaecol. Obstet.*, vol. 46, pp. 291–295, 1994.
- [39] W. Lammers, K. Arafat, A. El-Kays, and T. El-Sharkawy, "Spatial and temporal variation in local spike propagation in the myometrium of the 17-day pregnant rat," *Amer. J. Physiol. Cell. Physiol.*, vol. 267, pp. C1210–C1223, 1994.



Chiara Rabotti was born in Florence, Italy, in 1977. She received the M.Sc. degree in electrical engineering from the University of Florence, Florence, Italy, in 2004, and the Ph.D. degree from the Eindhoven University of Technology, Eindhoven, The Netherlands, in 2010.

Since 2010, she has been a Postdoctoral Fellow at the Signal Processing Systems Group, Eindhoven University of Technology. Her research interests include biomedical signal processing with specific focus on electrohysterography, electromyography, and

electrocardiography.

Dr. Rabotti is a member of the IEEE Engineering in Medicine and Biology Society.



Massimo Mischi was born in Rome, Italy, in 1973. He received the M.Sc. degree in electrical engineering from La Sapienza University, Rome, Italy, in 1999. In 2000, he joined as research Assistant at the Eindhoven University of Technology, Eindhoven, the Netherlands, where in 2002, he completed a two-year Post-Master program in technological design, information and communication technology, and in 2004, he received the Ph.D. degree.

His research focused on the development of cardiovascular diagnostic methods by contrast ultrasonography. Since 2007, he has been an Assistant Professor at the Eindhoven University of Technology. His current research interests include several topics in the area of biomedical signal processing.

Dr. Mischi is currently the Secretary of the Benelux Chapter of the IEEE Engineering in Medicine and Biology Society.



S. Guid Oei received the Ph.D. degree from the Leiden University, Leiden, The Netherlands, in 1996. He subspecialized in perinatology at Flinders University, Adelaide, Australia.

He is currently a Gynaecologist-Perinatologist in the Department of Obstetrics and Gynecology, Máxima Medical Center (MMC), Veldhoven, The Netherlands, where he has been the Dean and the Director of the Medical Simulation and Education Centre. He is also a Professor in fundamental perinatology in the Department of Electrical Engineering,

Eindhoven University of Technology, Eindhoven, The Netherlands.



Jan W. M. Bergmans (SM'91) received the degree of Elektrotechnisch Ingenieur (*cum laude*) in 1982, and the Ph.D. degree in 1987, both from Eindhoven University of Technology, Eindhoven, The Netherlands.

From 1982 to 1999, he was with Phillips Research Laboratories, Eindhoven, where he was involved in the signal-processing techniques and integrated circuit-architectures for digital transmission and recording systems. In 1988 and 1989, he was an Exchange Researcher at Hitachi Central Research

Laboratories, Tokyo, Japan. Since 1999, he has been a Professor and a Chairman of the Signal Processing Systems Group, Eindhoven University of Technology, and an Advisor at Phillips Research Laboratories. He is the author or coauthor of various refereed journals and is the author of the book *Digital Baseband Transmission and Recording* (Norwell, MA: Kluwer, 1996). He holds 40 U.S. patents.